SCONE: Surface Coverage Optimization in Unknown Environments by Volumetric Integration

Anonymous Author(s)
Affiliation
Address
email

Abstract

Next Best View computation (NBV) is a long-standing problem in robotics, and consists in identifying the next most informative sensor position(s) for reconstructing a 3D object or scene efficiently and accurately. Like most current methods, we consider here NBV prediction from a depth sensor. Methods relying on a volumetric representation of the scene are suitable for path planning, but do not scale well with the size of the scene and have lower accuracy than methods using a surface-based representation. However, the latter constrain the camera to a small number of poses. To obtain the advantages of both representations, we show that we can maximize surface metrics by Monte Carlo integration over a volumetric representation. Because our representation is based on a point cloud, our method scales to large scenes. Moreover, the camera can also move freely. We demonstrate our approach on a novel dataset made of large and complex 3D scenes.

1 Introduction

Next Best View computation (NBV) is a long-standing problem in robotics [6, 29], which consists in identifying the next most informative sensor position(s) for reconstructing a 3D object or scene efficiently and accurately. Typically, a position is evaluated on how much it can increase the total coverage of the scene surface. Few methods have relied on Deep Learning for the NBV problem, even though Deep Learning can provide useful geometric prior to obtain a better prediction of the surface coverage [33, 16, 25]. Like most current methods, we consider NBV prediction from a depth sensor. Existing methods based on a depth sensor rely either on a volumetric or on a surface-based representation of the scene geometry. Volumetric mapping-based methods can compute collision efficiently, which is practical for path planning in real case scenarios [20, 23, 24, 14, 1, 7]. However, they typically rely on voxels or a global embedding [12, 3, 21, 22, 27, 5] for the scene, which results in poor accuracy of the reconstructions and poor performance in NBV selection for complex 3D objects. On the contrary, surface mapping-based methods that process directly a dense point cloud of the surface as gathered by the depth sensor are efficient for NBV prediction with high-detailed geometry. They are however limited to very specific cases, generally a single, small-scale, isolated object floating in the air with the camera constrained to stay on a sphere centered on the object [15, 24, 8, 4, 13, 14, 14, 33, 16, 25]. Thus, they cannot be applied to the exploration of 3D scenes.

As shown in Figure 1, we introduce a volumetric Deep Learning method that efficiently identifies Next Best Views for unknown large-scale 3D scenes in which the camera can move freely. Instead of representing the scene with a single global embedding, we choose to use a grid of local point clouds, which scales much better to large and complex 3D scenes. We show how to learn to predict the visibility of new 3D points in all directions given an estimate of the 3D scene geometry. We can then integrate these visibilities in the direction of any camera by using a Monte Carlo integration

Submitted to 36th Conference on Neural Information Processing Systems (NeurIPS 2022). Do not distribute.

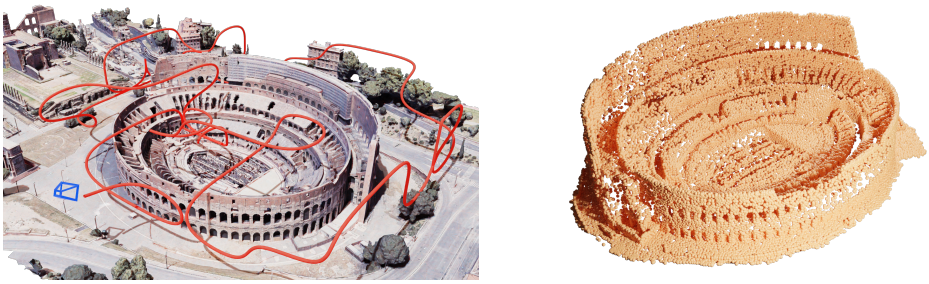

Figure 1: **Our Next Best View (NBV) method SCONE can handle unknown large-scale 3D scenes** to produce accurate 3D reconstruction inside a given 3D bounding box. Here, we call SCONE iteratively within a naive path planning algorithm to compute a complete camera trajectory avoiding collisions and obtain a complete 3D model. Despite being trained only on ShapeNet 3D models, it generalizes to complex scenes such as this one. (input 3D model courtesy of Brian Trepanier, under CC License. Downloaded from Sketchfab.)

approach, which allows us to optimize the camera pose to find the next most informative views. We call our method SCONE, for Surface Coverage Optimization in uNknown Environments.

In this respect, we introduce a theoretical framework to translate the optimization of surface coverage gain, a surface metric on manifolds that represents the ability of a camera to increase the visible area of the surface, into an optimization problem on volumetric integrals. Such a formalism allows us to use a volumetric mapping of geometry, which is convenient not only to scale the model to exploration tasks and scene reconstruction, but also to make probabilistic predictions about geometry.

In particular, given a partial point cloud gathered by a depth sensor, our model learns to make predictions with virtually infinite resolution about the occupancy probability in the scene volume by learning a deep implicit function [17, 28, 18, 30, 31, 19]. Such predictions scale to very large point clouds since they depend only on neighborhood geometry. Then, for each point, our model leverages a self-attention mechanism [26] to handle occlusions and learn information score functions mapped on a continuous sphere that represent visibility likelihood in all directions. The occupancy probability field is finally used as a basis to sample points and compute Monte Carlo integrals of visibility scores.

Since NBV learning-based methods are mostly limited to single, small-scale, centered object reconstruction in literature, we first compare the performance of our model to the state of the art on the ShapeNet dataset [2], following the protocol introduced in [33]. While our method was designed to handle more general frameworks such as 3D scene reconstruction and continuous cameras poses in the scene, it outperforms the state of the art for dense reconstruction of objects when the camera is constrained to stay on a sphere centered on the object.

We then conduct experiments in large 3D environments using a simple planning algorithm that builds a camera trajectory online by iteratively selecting NBVs with SCONE. Since, to the best of our knowledge, we propose the first supervised Deep Learning method for such free 6D motion of the camera, we created a dataset made of several large-scale scenes under the CC License for quantitative evaluation. We will make this dataset available for allowing comparison of future methods with SCONE.

2 Approach

As discussed in the introduction, our method relies on a volumetric representation of the object or scene to reconstruct because such a representation is useful for collision-free robot navigation. However, volumetric methods are generally less efficient to predict views that maximize dense surface metrics, because they dilute information in the 3D space with a sparser representation, *e.g.*, a voxel-based representation or a global encoding, and thus suffer from a loss in resolution.

To overcome this problem, we first show that we can maximize a surface metric by integrating over a volumetric representation. As we argue below, this integration over a volume is much more efficient for optimizing surface coverage gain than the alternative of identifying the 3D points lying on the

surface, which is difficult in an unknown and occluded environment. More exactly, we derive a volumetric integral that is asymptotically proportional to the surface metric, which is enough for our maximization problem. We first present this derivation considering volume represented as a perfect binary occupancy map. We then turn to a probabilistic version of the occupancy map, as this maps is not perfectly known at run-time.

We finally explain how we predict the different terms involved in the volumetric integration by leveraging neural models and self-attention mechanisms to predict unknown geometry and handle occlusions.

2.1 Maximizing Surface Coverage Gain on a Binary Occupancy Map

Here, we consider a binary occupancy map $\sigma : \mathbb{R}^3 \to \{0, 1\}$ representing the volume of the target object or scene. We will relax our derivations to a probabilistic occupancy map when looking for the next best view in the next subsections. From the binary map σ, we can define the set χ of occupied points, *i.e.*, the set of points x verifying $\sigma(x) = 1$, its surface as the boundary $\partial\chi$, and the surface coverage $C(c)$ achieved by a camera pose $c = (c_{\text{pos}}, c_{\text{rot}}) \in \mathcal{C} := \mathbb{R}^3 \times SO(3)$ as the following surface integral:

$$C(c) = \frac{1}{|\partial\chi|_S} \int_{\partial\chi} \mathbb{1}_{\chi_c}(x) \cdot v_c(x) \, \mathrm{d}x, \tag{1}$$

where $|\partial\chi|_S := \int_{\partial\chi} \mathrm{d}x$ is the area of surface $\partial\chi$. $\chi_c \subset \chi$ is the subset of occupied points contained in the field of view of camera c, and $v_c(x)$ is the visibility of point x, *i.e.*, $v_c(x) = \mathbb{1}\left(\sigma\left(\{(1-\lambda)c_{\text{pos}} + \lambda x \text{ such that } \lambda \in [0, 1)\}\right) = \{0\}\right)$.

Since we want to maximize the total coverage of the surface by all cameras during reconstruction, we are actually interested in maximizing the coverage of previously unobserved points rather than the absolute coverage. Given a set of previous camera poses, which we call the *camera history* $H \subset \mathcal{C}$, and a 3D point x, we introduce the *knowledge factor* $\gamma_H : \mathbb{R}^3 \to \{0, 1\}$ such that $\gamma_H(x) = \max\{v_c(x) : c \in H\}$. We then define the *coverage gain* $G_H(c)$ of camera pose c as:

$$G_H(c) = \frac{1}{|\partial\chi|_S} \int_{\partial\chi} \mathbb{1}_{\chi_c}(x) \cdot \nu_c^H(x) \, \mathrm{d}x, \tag{2}$$

where $\nu_c^H(x) = (1 - \gamma_H(x)) \cdot v_c(x)$ is the *visibility gain* of x in χ_c, for camera history H. This function is equal to 1 iff x is visible at pose c but was not observed by any camera pose in H. Given a camera history H, our goal is to identify a pose c that maximizes $G_H(c)$.

Given an occupancy map σ, we could evaluate the integral in Eq. (2) by simply sampling points p on surface $\partial\chi$. However, this would not be efficient as it is difficult to identify which points x are on $\partial\chi$ from σ, especially in unknown environments. It is thus not possible to directly maximize $G_H(c)$. Instead, we extend the properties of surface points to a small tubular neighborhood of the surface. This will allow us to replace the maximization of a surface metric by the maximization of a volumetric integral, which is much easier to compute from our volumetric representation.

More exactly, we suppose that there exists a small quantity $\mu_0 > 0$ such that any volume point in the tubular neighborhood $T(\partial\chi, \mu_0) := \left\{p \in \mathbb{R}^3 \mid \exists x \in \partial\chi, \|x - p\|_2 < \mu_0\right\}$ keeps the same visibility property as its neighboring surface points. With such a hypothesis, we give a thickness to the surface, which makes sense when working with discrete points sampled in space to approximate a volume.

To this end, we introduce a new visibility gain function $\overline{\nu}_c^H$ to adapt the definition of the former visibility gain ν_c^H. For any $0 < \mu < \mu_0$:

$$\overline{\nu}_c^H(\mu; x) = \begin{cases} 1 & \text{if } \exists x_0 \in \partial\chi, \lambda < \mu \text{ such that } x = x_0 + \lambda N(x_0) \text{ and } \nu_c^H(x_0) = 1, \\ 0 & \text{otherwise ,} \end{cases} \tag{3}$$

where N is the inward normal vector field. With further regularity assumptions about the surface that are detailed in the supplementary material, such quantities are well defined. Assuming μ_0 is small enough, the following explicit formula translates the surface approach into a volume integral for any camera pose $c \in \mathcal{C}$ and $\mu < \mu_0$:

$$\int_{T(\partial\chi,\mu)} g_c^H(\mu; x) \mathrm{d}x = \int_{\partial\chi} \int_{-\mu}^{\mu} g_c^H(\mu; x_0 + \lambda N(x_0)) \, \det(I - \lambda W_{x_0}) \, \mathrm{d}\lambda \, \mathrm{d}x, \tag{4}$$

with $g_c^H(\mu,\cdot) : x \mapsto \mathbb{1}_{\chi_c}(x) \cdot \overline{\nu}_c^H(\mu;x)$ and W_{x_0} the Weingarten map at x_0, that is, the Hessian of the signed distance function on the boundary of χ, which is continuous on the scene surface, assumed to be compact [10].

By developing the determinant, we find that $\det(I - \lambda W_{x_0}) = 1 + \lambda b(\lambda, x_0)$ where b is a bounded function on the compact space $[-\mu,\mu] \times \partial\chi$. Moreover, for all $x_0 \in \partial\chi$, we have by definition $g_c^H(\mu; x_0+\lambda N(x_0)) = g_c^H(\mu; x_0) = \mathbb{1}_{\chi_c}(x_0)\cdot\nu_c(x_0)$ when $0 \leq \lambda < \mu$, and $g_c^H(\mu; x_0+\lambda N(x_0)) = 0$ when $-\mu < \lambda < 0$. It follows that, for every $0 < \mu < \mu_0$:

$$\begin{aligned}\int_{T(\partial\chi,\mu)} g_c^H(\mu;x)\mathrm{d}x &= \int_{\partial\chi}\int_0^\mu g_c^H(\mu;x_0)(1+\lambda b(\lambda,x_0))\,\mathrm{d}\lambda\,\mathrm{d}x_0 \\ &= \mu\int_{\partial\chi} g_c^H(\mu;x_0)\,\mathrm{d}S_{x_0} + \int_{\partial\chi}\int_0^\mu \lambda g_c^H(\mu;x_0)b(\lambda,x_0)\,\mathrm{d}\lambda\,\mathrm{d}x_0 \qquad (5)\\ &= \mu|\partial\chi|_S G_H(c) + \int_{\partial\chi}\int_0^\mu \lambda g_c^H(\mu;x_0)b(\lambda,x_0)\,\mathrm{d}\lambda\,\mathrm{d}x_0.\end{aligned}$$

The complete derivations are given in the supplementary material.

Since the volume is supposed to be opaque, function $g_c^H(\mu;\cdot)$ is equal to 0 for every point outside $T(\partial\chi,\mu)$. Moreover, considering the regularity assumptions we made on the compact surface, if μ_0 is chosen small enough then for all $x_0 \in \partial\chi, \mu < \mu_0$, the point $x_0 + \mu N(x_0)$ is located inside the volume, such that $\int_{T(\partial\chi,\mu)} g_c^H(\mu;x)\,\mathrm{d}x = \int_\chi g_c^H(\mu;x)\,\mathrm{d}x$.

Since $|g_c^H(\mu;\cdot)| \leq 1$ for all $c \in \mathcal{C}$ and $\mu > 0$, we deduce the following theorem by bounding $|b|$ on $[-\mu,\mu] \times \partial\chi$:

Theorem 1 *Under the previous regularity assumptions on the volume χ of the scene and its surface $\partial\chi$, there exist $\mu_0 > 0$ and $M > 0$ such that for all $\mu < \mu_0$, and any camera $c \in \mathcal{C}$:*

$$\left|\frac{1}{|\chi|_V}\int_\chi g_c^H(\mu;x)dx - \mu\frac{|\partial\chi|_S}{|\chi|_V}G_H(c)\right| \leq M\mu^2\ , \qquad (6)$$

where $|\chi|_V$ is the volume of χ.

This theorem states that, asymptotically for small values of μ, the volume integral $\int_\chi g_c^H(\mu;x)\,\mathrm{d}x$ gets proportional to the surface coverage gain values $G_H(c)$ that we want to maximize. This result is convenient since a volume integral can be easily approximated with Monte-Carlo integration on the volume and a uniform dense sampling based on the occupancy function σ. Consequently, the more points we sample in the volume, the smaller μ we can choose, and the closer maximizing the volume integral of tubular neighborhood visibility gain gets to maximizing the surface coverage gain.

2.2 Architecture

To handle unknown environments, our model is split into two modules. The first one focuses on geometry and learns to predict the occupancy map σ as an occupancy probability field $\hat{\sigma}$. The second module uses this predicted occupancy field to estimate the visibility gain functions $\nu_{\chi_c}^H$, which is ultimately used to compute the coverage gain with Monte Carlo integration.

Predicting the occupancy probability field $\hat{\sigma}$. The occupancy function σ is not known perfectly in practice. We thus approximate σ with the first module of our model, which consists of a deep neural network $\hat{\sigma} : \mathcal{P}(\mathbb{R}^3) \times \mathbb{R}^3 \to [0,1]$ that takes as inputs a partial point cloud $P_H \subset \mathbb{R}^3$ as well as query points $x \in \mathbb{R}^3$, and outputs the occupancy probability $\hat{\sigma}(P_H;x)$. P_H is obtained by merging together all depth maps previously captured from cameras in H.

As shown in Figure 2, rather than using a direct encoding of the global shape of P_H as input to $\hat{\sigma}$, we take inspiration from [9] to achieve scalability and encode P_H using features computed from the points' neighborhoods. The difference with [9] is that we rely on a multiscale approach: For a given query 3D point x, these features are computed from the k nearest neighbors of x computed at different scales. For each scale s, we downsample point cloud P_H around x into a sparser point cloud $P_H^{(s)}$ before recomputing the nearest neighbors $p_i^{(s)}(x), i = 1, ..., k$ of x: In this way, the size of the neighborhood increases with scale.

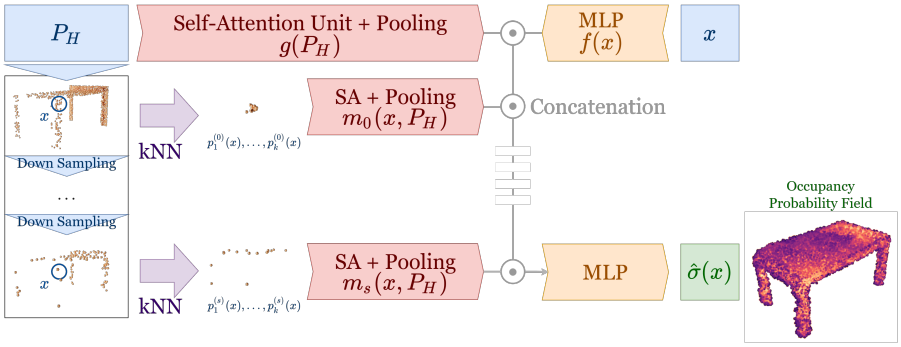

Figure 2: **Architecture of the first module of SCONE**, which predicts the occupancy probability field $\hat{\sigma}$. This module predicts the occupancy probability of a point x from three types of inputs: The point x after transformation by an MLP $f(x)$; A coarse global encoding $g(P_H)$ of the point cloud obtained by applying self-attention units on the sequence of points followed by a pooling operation; Multi-scale neighborhood features $m_i(x, P_H), i = 0, ..., N$ computed by down-sampling multiple times the point cloud, and encoding the k nearest neighbors of x with self-attention units after each sampling.

Next, for each value of s, we use small attention units [26, 11] on the sequence of centered neighborhood points $(p_1^{(s)}(x) - x, ..., p_k^{(s)}(x) - x)$ and apply pooling operations to encode each sequence of k neighbors into a single feature that describes the local geometry for the corresponding scale. We finally concatenate these different scale features with another uncentered global feature as well as the query point x, and feed them to an MLP to predict the occupancy probability. The last global feature aims to provide really coarse information about the geometry and the location of x in the scene.

This model scales well to large scenes: Adding points from distant views to the current partial point cloud does not change the local state of the point cloud. To avoid computing neighborhoods on the entire point cloud when reconstructing large scenes, we partition the space into cells in which we store the points in P_H. Then, given a query point x, we only use the neighboring cells to compute $p_i^{(s)}(x), i = 1, ..., k$.

Predicting the visibility gain $\nu_{\chi_c}^H$. To maximize the surface coverage gain, we need to compute the volumetric integral of the visibility gain functions $\nu_{\chi_c}^H$. We do this again by Monte Carlo sampling, however, in unknown environments we cannot compute explicitly occlusions to derive visibility gain functions $\nu_{\chi_c}^H$ since the geometry, represented as a point cloud, is partially unknown and sparser than a true surface. We thus train the second module of our model to predict the visibility gain functions by leveraging a self-attention mechanism that implicitly helps to estimate occlusion effects in the discrete point cloud P_H.

In particular, for any camera pose $c \in \mathcal{C}$ and 3D point $x \in \chi_c$, the second module derives its prediction of visibility gains from three core features: (i) The predicted probability $\hat{\sigma}(P; x)$ of x to be occupied, (ii) the occlusions on x by the subvolume χ_c and (iii) the camera history H. To feed all this information to our model in an efficient way, we follow the pipeline presented in Figure 3. The model starts by using the predicted occupancy probability function $\hat{\sigma}$ to sample 3D points in the volume χ. These samples will be used for Monte Carlo integration. We refer to these points as *proxy points* as we use them to encode the volume in the camera field of view, *i.e.*, in a pyramidal frustum view. We write $\hat{\chi}$ as the discrete set of sampled proxy points, and $\hat{\chi}_c$ as the set of proxy points located in the field of view of the camera c.

We first encode these proxy points individually by applying a small MLP on their 3D coordinates and their occupancy probability value concatenated together. Then, our model processes the sequence of these encodings with a self-attention unit to handle occlusion effects of subvolume χ_c on every individual point. Note there is no pooling operation on the output of this unit: The network predicts per-point features and does not aggregate predictions, since we do it ourselves with Monte Carlo integration. Next, for each proxy point $x \in \hat{\chi}$, we compute an additional feature $h_H(x)$ that encodes the history of camera positions H with respect to this point as a spherical mapping: It consists in

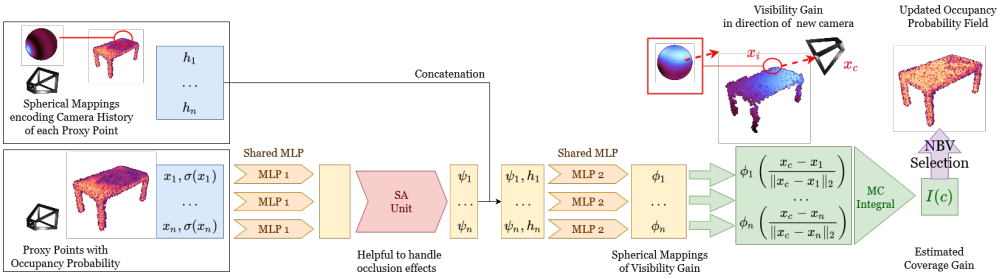

Figure 3: **Architecture of the second part of SCONE**, which predicts a visibility gain for each proxy point. To make this prediction, the model encodes the proxy points x concatenated with their occupancy probability $\hat{\sigma}(x)$. We use an attention mechanism to take into account occlusion effects in the volume between the proxy points and its consequences on the visibility gains.

the projection on a sphere centered on x of all camera positions for which x was in the field of view. These features are concatenated to the outputs of the self-attention unit.

Our model finally uses an MLP on these features to predict the entire visibility gain functions of every point x as a vector of coordinates in the orthonormal basis of spherical harmonics. With such a formalism, the model is able to compute visibility gains for points inside a subvolume in all directions with a single forward pass. In this regard, we avoid unnecessary computation and are able to process a large number of cameras in the same time when they share the same proxy points in their field of view (*e.g.*, reconstruction of a single object centered in the scene, where $\hat{\chi}_c = \hat{\chi}$ for all c, or when several cameras observe the same part of the 3D scene, *i.e.*, $\hat{\chi}_c = \hat{\chi}' \subset \hat{\chi}$ for several c).

Formally, if we denote by $Y_l^m : S^2 \to \mathbb{R}$ the real spherical harmonic of rank (l, m) and $\phi_l^m(\hat{\chi}_c; x, h_H(x))$ the predicted coordinate of rank (l, m) for proxy point $x \in \hat{\chi}_c$ with attention to subset $\hat{\chi}_c$ and camera history feature $h_H(x)$, the visibility gain of point x in direction $d \in S^2$ is defined as

$$\sum_{l,m} \phi_l^m(\hat{\chi}_c; x, h_H(x)) \cdot Y_l^m(d) \tag{7}$$

so that the coverage gain $G_H(c)$ of a camera pose $c \in \mathcal{C}$ is proportional to

$$I_H(c) := \frac{1}{|\hat{\chi}|} \sum_{x \in \hat{\chi}} \left[\mathbb{1}_{\hat{\chi}_c}(x) \sum_{l,m} \phi_l^m(\hat{\chi}_c; x, h_H(x)) \cdot Y_l^m\left(\frac{x - c_{pos}}{\|x - c_{pos}\|_2} \right) \right]. \tag{8}$$

The next best view among several camera positions is finally defined as the camera pose c^* with the highest value for $I_H(c^*)$.

We also use spherical harmonics to encode the camera history encoding $h_H(x)$ of each point x, which makes it a homogeneous input to the predicted output. Consequently, this input comes at the end of the architecture, and aims to adapt the visibility gain according to previous camera positions. This convenient representation, inspired by [32], allows us to handle free camera motion; On the contrary, several models in the literature encode the camera directions on a discrete sphere [33, 16, 25].

Training. We train the occupancy probability module alone with a Mean Squared Error loss with the ground truth occupancy map. We do not compute ground-truth visibility gains to train the second module since it would make computation more difficult and require further assumptions: We supervise directly on $I_H(c)$ by comparing it to the ground-truth surface coverage gain for multiple cameras, with softmax normalization and Kullback-Leibler divergence loss. Extensive details about the training of our modules and the choices we made are given in the supplementary material.

3 Experiments

As discussed in the introduction, deep learning-based NBV models for dense reconstruction are currently limited to single, small-scale, centered object reconstruction. To compare SCONE to these previous methods in this context, we first constrain the camera pose to lie on a sphere centered on

Table 1: **AUCs of surface coverage for several NBV selection methods for dense object reconstruction**, as computed on the ShapeNet test dataset following the protocol of [33], and after averaging over multiple seeds in the case of our method. For this experiment, we constrain the camera to stay on a sphere centered on the objects in order to compare with previous methods. Even if our model is designed to scale to entire scene reconstructions with free camera motion, it is still able to beat other methods trained for the specific case of dense object reconstruction with constrained camera motion.

	Categories seen during training								
Method	Airplane	Cabinet	Car	Chair	Lamp	Sofa	Table	Vessel	Mean
Random	0.745	0.545	0.542	0.724	0.770	0.589	0.710	0.674	0.662
Proximity Count [8]	0.800	0.596	0.591	0.772	0.803	0.629	0.753	0.706	0.706
Area Factor [23]	0.797	0.585	0.587	0.751	0.801	0.627	0.725	0.714	0.698
NBV-Net [16]	0.778	0.576	0.596	0.743	0.791	0.599	0.693	0.667	0.680
PC-NBV [33]	0.799	0.612	**0.612**	**0.782**	0.800	0.640	0.760	0.719	0.716
SCONE (Ours)	**0.827**	**0.625**	0.591	**0.782**	**0.819**	**0.662**	**0.792**	**0.734**	**0.729**

	Categories not seen during training								
Method	Bed	Bench	Bookshelf	Bus	Guitar	Motorbike	Pistol	Skateboard	Mean
Random	0.609	0.619	0.695	0.795	0.795	0.672	0.768	0.614	0.694
Proximity Count	0.646	0.645	**0.749**	0.829	0.854	0.705	0.828	0.660	0.740
Area Factor	0.629	0.631	0.742	0.827	0.852	0.718	0.799	0.660	0.732
NBV-Net	0.654	0.628	0.729	0.824	0.834	0.710	0.825	0.645	0.731
PC-NBV	0.667	0.662	0.740	**0.845**	0.849	**0.728**	0.840	0.672	0.750
SCONE (Ours)	**0.694**	**0.689**	0.746	0.832	**0.860**	**0.728**	**0.845**	**0.717**	**0.764**

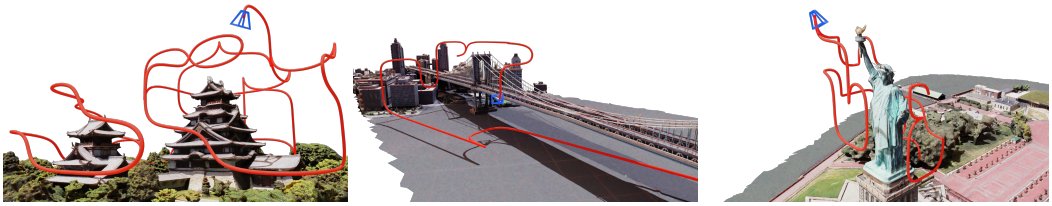

Figure 4: **Application of our NBV approach to the reconstruction of large 3D structures**. The path, constructed iteratively in real time with our method, is shown in red.

an object. We then introduce our dataset made of large-scale 3D models that we created to evaluate SCONE on free camera motions.

3.1 Next Best View for Single Object Reconstruction

We first compare the performance of our model to the state of the art on a subset of the ShapeNet dataset [2] introduced in [33] and following the protocol of [33]: We sample 4,000 training meshes from 8 specific categories of objects, 400 validation meshes and 400 test meshes from the same categories, and 400 additional test meshes from 8 categories unseen during training.

The evaluation on the test datasets consists of 10-view reconstructions of single objects. Given a mesh in the dataset, camera positions are discretized on a sphere. We start the reconstruction process by selecting a random camera pose, then we iterate NBV selection 9 times in order to maximize coverage with a sequence of 10 views in total. The evaluation metric is the area under the curve (AUC) of surface coverage throughout the reconstruction. This criterion not only evaluates the quality of final surface coverage, but also the convergence speed toward a satisfying coverage. Results are presented in Table 1. Further details about the evaluation and the metric computation are available in the supplementary material.

Method	3D scene				
	Colosseum	Statue of Liberty	Manhattan Bridge	Fushimi Castle	Mean
Random Walk	0.309	0.369	0.374	0.513	0.391
SCONE-Entropy	0.514	0.679	0.381	0.819	0.598
SCONE	**0.583**	**0.689**	**0.602**	**0.839**	**0.678**

(a)

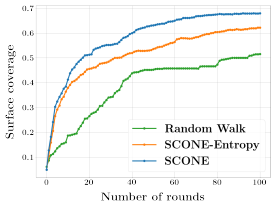

(b)

Figure 5: **(a) AUCs of surface coverage for several NBV selection methods during active view planning experiments on several 3D scenes from our dataset.** Results are averaged on several trajectories. **(b) Surface coverage curves for the different NBV selection methods, averaged on all 3D scenes.** Despite being trained only on centered ShapeNet 3D models, the second module of SCONE is able to generalize to complex scenes when predicting the visibility scores.

3.2 Active View Planning in a 3D Scene

To evaluate the scalability of our model to large environments as well as free camera motion in 3D space, we also conducted experiments using a naive planning algorithm that incrementally builds a path in the scene: For this algorithm, we first discretize the camera poses in the scene on a 5D grid, corresponding to coordinates $c_{pos} = (x_c, y_c, z_c)$ of the camera as well as the elevation and azimuth to encode rotation c_{rot}. The number of poses depends on the dimensions of the bounding box of the scene. This bounding box is an input to the algorithm, as a way for the user to tell which part of the scene should be reconstructed. In our experiments, the number of different poses is around 10,000. Note we did not retrain our model for such scenes and use the previous model trained on ShapeNet as explained in Section 3.1.

The depth sensor starts from a random pose (from which, at least, a part of the main structure to reconstruct is visible). Then, at each iteration, our method estimates the coverage gain of direct neighboring poses in the 5D grid, and selects the one with the highest score. The sensor moves to this position, captures a new partial point cloud and concatenates it to the previous one. Since we focus on online path planning for dense reconstruction optimization and designed our model to be scalable with local neighborhood features, the size of the global point cloud can become very large. We iterate the process either 50 or 100 times to build a full path around the object in around 5 minutes on a single Nvidia GTX1080 GPU, and recovered a partial point cloud with up to 100,000 points.

Contrary to single, small-scale object reconstruction where the object is always entirely included in the field of view, we simulated a limited range in terms of field of view and depth for the depth sensor, so that the extent of the entire scene cannot be covered in a single view. Thus, taking pictures at long range and going around the scene randomly is not an efficient strategy; the sensor must find a path around the surface to optimize the full coverage. We use a ray-tracing renderer to capture the partial point cloud to approximate a real Lidar. More details about the experiments can be found in the supplementary material.

We compared the performance of SCONE with simple baselines: First, a random walk, which chooses neighboring poses randomly with uniform probabilities. Then, we evaluated an alternate version of our model, which we call SCONE-Entropy, which leverages the first module of our full model to compute occupancy probability in the scene, then selects the next best view as the position that maximizes the Shannon entropy in its field of view. The comparison is interesting, since SCONE-Entropy adapts classic NBV approaches based on information theory to a deep learning framework. Quantitative results are available in Table 5(a).

Despite being trained only on ShapeNet 3D models, our method is able to compute meaningful paths around the structures and consistently reach satisfying global coverage. Since we focused on building a metric for NBV computation, this experiment is simple and does not implement any further prior from common path planning strategies: For instance, we do not compute distant NBV, nor optimal paths to move from a position to a distant NBV with respect to our volumetric mapping. There is no doubt the model could benefit from further strategies inspired by the path planning literature.

Architecture	Mean Squared Error
Base Architecture	0.0397
No Neighborhood Feature	0.0816
With Camera History	**0.0386**

(a) Occupancy probability

Architecture	Kullback-Leibler Divergence
Base Architecture	**0.00039**
No prediction $\hat{\sigma}$	0.00051
No Camera History	0.00045

(b) Coverage gain

Figure 6: **(a) Comparison of Mean Squared Error for variations of our occupancy probability prediction model. (b) Comparison of Kullback-Leibler divergence for variations of our coverage gain computation model.** Thanks to the volumetric prediction $\hat{\sigma}$, the full model predicts a better distribution of coverage gains on the whole space as it is indicated by KL divergence, which is convenient for full path planning in a 3D scene.

3.3 Ablation Study

We now provide an ablation study for both modules of our full model: The prediction of occupancy probability, and the computation of coverage gain from predictions about visibility gains. To evaluate both modules separately, we compared their performance on their training critera: Mean-Squared Error for occupancy probability prediction, and softmax followed by Kullback-Leibler divergence on a dense set of cameras for coverage gain. The values are reported in Figure 6. We also provide further analysis in the supplementary material.

Occupancy probability. Apart from the base architecture presented in Figure 2, we trained the occupancy probability prediction module under two additional settings. First, we removed the multi-scale neighborhood features computed by downsampling the partial point cloud P_H, and trained the module to predict an occupancy probability value $\hat{\sigma}$ only from global feature $g(P_H)$ and encoding $f(x)$. As anticipated, the lack of neighborhood features not only prevents the model from an efficient scaling to large scenes, but also causes a huge loss in performance. We also trained a slightly more complex version of our occupancy probability prediction module by feeding it the spherical mappings $h_H(x)$ of camera history H as an additional feature. It appears this helps the model to increase its confidence and make better predictions, but the gains are quite marginal. Extensive details are provided in the supplementary material.

Visibility gain. We trained two variations of our visibility gain prediction module. In the first one, we completely removed the geometric prediction: We use directly the surface points as proxy points, mapped with an occupancy probability equal to 1. As a consequence, the model suffers from a significant loss in performance to compute coverage gain from its predicted visibility gain functions. Thus, we can confirm that the volumetric framework improves the performance of SCONE. This result is remarkable, since models that rely on surface point clouds usually make better NBV predictions for dense reconstruction of detailed objects in literature. On the contrary, we show that our formalism is able to achieve higher performance by leveraging a volumetric representation with a high resolution deep implicit function $\hat{\sigma}$. We trained a second variation without the spherical mappings h_H of camera history. We verified that such additional features increase performance, especially at the end of a 3D reconstruction.

4 Limitations and Conclusion

Beyond the prediction of the Next Best View, our method SCONE is able to evaluate the value of any camera pose given a current estimate of the scene volume. We demonstrated this ability with a simple path planning algorithm that looks for the next pose around the current pose iteratively. However:

- Like current methods, SCONE relies on a depth sensor and assumes that the captured depth maps are perfect. In practice, such a sensor is not necessarily available and can also be noisy. It would be very interesting to extend the approach to color cameras.
- Also like current methods, it is limited to the prediction of the camera pose for the next step. This is a greedy, non-necessarily optimal as multiple camera poses are required anyway for a complete 3D reconstruction. We believe that, thanks to its scalability, our method could be extended to the prediction of the "Next Best Path", where the future camera poses would be predicted jointly for their complementarity.

References

[1] Fredrik Bissmarck, Martin Svensson, and Gustav Tolt. Efficient Algorithms for Next Best View Evaluation. In *International Conference on Intelligent Robots and Systems*, 2015.

[2] Angel X. Chang, Thomas Funkhouser, Leonidas Guibas, Pat Hanrahan, Qixing Huang, Zimo Li, Silvio Savarese, Manolis Savva, Shuran Song, Hao Su, Jianxiong Xiao, Li Yi, and Fisher Yu. ShapeNet: An Information-Rich 3D Model Repository. Technical report, Stanford University, Princeton University, Toyota Technological Institute at Chicago, 2015.

[3] Benjamin Charrow, Gregory Kahn, Sachin Patil, Sikang Liu, Kenneth Goldberg, Pieter Abbeel, Nathan Michael, and Vijay Kumar. Information-Theoretic Planning with Trajectory Optimization for Dense 3D Mapping. In *Robotics: Science and Systems*, 2015.

[4] S.Y. Chen and Youfu Li. Vision Sensor Planning for 3–D Model Acquisition. *IEEE Transactions on Systems, Man, and Cybernetics*, 2005.

[5] Titus Cieslewski, Elia Kaufmann, and Davide Scaramuzza. Rapid Exploration with Multi-Rotors: A Frontier Selection Method for High Speed Flight. In *International Conference on Intelligent Robots and Systems*, 2017.

[6] C. Ian Connolly. The Determination of Next Best Views. In *International Conference on Robotics and Automation*, 1985.

[7] Jonathan Daudelin and Mark Campbell. An Adaptable, Probabilistic, Next Best View Algorithm for Reconstruction of Unknown 3D Objects. *IEEE Robotics and Automation Letters*, 2017.

[8] Jeffrey Delmerico, Stefan Isler, Reza Sabzevari, and Davide Scaramuzza. A Comparison of Volumetric Information Gain Metrics for Active 3D Object Reconstruction. *Autonomous Robots*, 2018.

[9] Philipp Erler, Paul Guerrero, Stefan Ohrhallinger, Michael Wimmer, and Niloy J. Mitra. Points2Surf: Learning Implicit Surfaces from Point Cloud Patches. *European Conference on Computer Vision*, 2020.

[10] David Gilbarg and Neil S. Trudinger. *Elliptic Partial Differential Equations of Second Order*. Classics in Mathematics. Springer Berlin Heidelberg, 2001.

[11] Meng-Hao Guo, Junxiong Cai, Zheng-Ning Liu, Tai-Jiang Mu, Ralph R. Martin, and Shi-Min Hu. PCT: Point Cloud Transformer. *Computational Visual Media*, 2020.

[12] Benjamin Hepp, Debadeepta Dey, Sudipta N. Sinha, Ashish Kapoor, Neel Joshi, and Otmar Hilliges. Learn-to-Score: Efficient 3D Scene Exploration by Predicting View Utility. In *European Conference on Computer Vision*, 2018.

[13] Simon Kriegel, Tim Bodenmüller, Michael Suppa, and Gerd Hirzinger. A Surface-Based Next-Best-View Approach for Automated 3D Model Completion of Unknown Objects. In *International Conference on Robotics and Automation*, 2011.

[14] Simon Kriegel, Christian Rink, Tim Bodenmüller, Alexander Narr, Michael Suppa, and Gerd Hirzinger. Next-Best-Scan Planning for Autonomous 3D Modeling. *International Conference on Intelligent Robots and Systems*, 2012.

[15] Inhwan Dennis Lee, Ji Hyun Seo, Young Min Kim, Jonghyun Choi, Soonhung Han, and Byounghyun Yoo. Automatic Pose Generation for Robotic 3-D Scanning of Mechanical Parts. *IEEE Transactions on Robotics and Automation*, 2020.

[16] Miguel Mendoza, Juan Irving Vasquez-Gomez, Hind Taud, Luis Enrique Sucar, and Carolina Reta. Supervised Learning of the Next-Best-View for 3D Object Reconstruction. *Computing Research Repository*, 2019.

[17] Lars M. Mescheder, Michael Oechsle, Michael Niemeyer, Sebastian Nowozin, and Andreas Geiger. Occupancy Networks: Learning 3D Reconstruction in Function Space. *International Conference on Computer Vision and Pattern Recognition*, 2019.

[18] Ben Mildenhall, Pratul P. Srinivasan, Matthew Tancik, Jonathan T. Barron, Ravi Ramamoorthi, and Ren Ng. NeRF: Representing Scenes as Neural Radiance Fields for View Synthesis. *European Conference on Computer Vision*, 2020.

[19] Michael Oechsle, Songyou Peng, and Andreas Geiger. UNISURF: Unifying Neural Implicit Surfaces and Radiance Fields for Multi-View Reconstruction. *International Conference on Computer Vision*, 2021.

[20] Christian Potthast and Gaurav Sukhatme. A Probabilistic Framework for Next Best View Estimation in a Cluttered Environment. *Journal of Visual Communication and Image Representation*, 2014.

[21] Soohwan Song and Sungho Jo. Online Inspection Path Planning for Autonomous 3D Modeling using a Micro-Aerial Vehicle. In *International Conference on Robotics and Automation*, 2017.

[22] Soohwan Song, Daekyum Kim, and Sungho Jo. Online Coverage and Inspection Planning for 3D Modeling. *Autonomous Robots*, 2020.

[23] Juan Vasquez-Gomez, Luis Sucar, Rafael Murrieta-Cid, and Efrain Lopez-Damian. Volumetric Next-Best-View Planning for 3D Object Reconstruction with Positioning Error. *International Journal of Advanced Robotic Systems*, 2014.

[24] Juan Vasquez-Gomez, Luis Sucar, and Rafael Murrieta-Cid. View/State Planning for Three-Dimensional Object Reconstruction under Uncertainty. *Autonomous Robots*, 2017.

[25] Juan Vasquez-Gomez, David Troncoso Romero, Israel Becerra, Luis Sucar, and Rafael Murrieta-Cid. Next-best-view Regression using a 3D Convolutional Neural Network. *Machine Vision and Applications*, 2021.

[26] Ashish Vaswani, Noam Shazeer, Niki Parmar, Jakob Uszkoreit, Llion Jones, Aidan N. Gomez, Lukasz Kaiser, and Illia Polosukhin. Attention Is All You Need. *Advances in Neural Information Processing Systems*, 2017.

[27] Chaoqun Wang, Han Ma, Weinan Chen, Li Liu, and Max Meng. Efficient Autonomous Exploration With Incrementally Built Topological Map in 3-D Environments. *Transactions on Instrumentation and Measurement*, 2020.

[28] Qiangeng Xu, Weiyue Wang, Duygu Ceylan, Radomír Mech, and Ulrich Neumann. DISN: Deep Implicit Surface Network for High-quality Single-view 3D Reconstruction. *Advances in Neural Information Processing Systems*, 2019.

[29] Brian Yamauchi. A Frontier-Based Approach for Autonomous Exploration. In *International Conference on Robotics and Automation*, 1997.

[30] Lior Yariv, Matan Atzmon, and Yaron Lipman. Universal differentiable renderer for implicit neural representations. *arXiv Preprint*, 2020.

[31] Lior Yariv, Jiatao Gu, Yoni Kasten, and Yaron Lipman. Volume Rendering of Neural Implicit Surfaces. *Advances in Neural Information Processing Systems*, 2021.

[32] Alex Yu, Sara Fridovich-Keil, Matthew Tancik, Qinhong Chen, Benjamin Recht, and Angjoo Kanazawa. Plenoxels: Radiance Fields without Neural Networks. *International Conference on Computer Vision and Pattern Recognition*, 2022.

[33] Rui Zeng, Wang Zhao, and Yong-Jin Liu. PC-NBV: A Point Cloud Based Deep Network for Efficient Next Best View Planning. In *International Conference on Intelligent Robots and Systems*, 2020.

Checklist

1. For all authors...
   (a) Do the main claims made in the abstract and introduction accurately reflect the paper's contributions and scope? [Yes]
   (b) Did you describe the limitations of your work? [Yes] See the last section.
   (c) Did you discuss any potential negative societal impacts of your work? [Yes] A discussion can be found in the supplementary material.
   (d) Have you read the ethics review guidelines and ensured that your paper conforms to them? [Yes]
2. If you are including theoretical results...
   (a) Did you state the full set of assumptions of all theoretical results? [Yes]
   (b) Did you include complete proofs of all theoretical results? [Yes]
3. If you ran experiments...
   (a) Did you include the code, data, and instructions needed to reproduce the main experimental results (either in the supplemental material or as a URL)? [No] Not yet, but we will release our source code and dataset.
   (b) Did you specify all the training details (e.g., data splits, hyperparameters, how they were chosen)? [Yes] In the supplementary material.
   (c) Did you report error bars (e.g., with respect to the random seed after running experiments multiple times)? [No]
   (d) Did you include the total amount of compute and the type of resources used (e.g., type of GPUs, internal cluster, or cloud provider)? [Yes] See supplementary material.
4. If you are using existing assets (e.g., code, data, models) or curating/releasing new assets...
   (a) If your work uses existing assets, did you cite the creators? [Yes]
   (b) Did you mention the license of the assets? [Yes]
   (c) Did you include any new assets either in the supplemental material or as a URL? [No]
   (d) Did you discuss whether and how consent was obtained from people whose data you're using/curating? [Yes]
   (e) Did you discuss whether the data you are using/curating contains personally identifiable information or offensive content? [No] Our data do not have such issue.
5. If you used crowdsourcing or conducted research with human subjects...
   (a) Did you include the full text of instructions given to participants and screenshots, if applicable? [N/A]
   (b) Did you describe any potential participant risks, with links to Institutional Review Board (IRB) approvals, if applicable? [N/A]
   (c) Did you include the estimated hourly wage paid to participants and the total amount spent on participant compensation? [N/A]